

UniFixer: A Universal Reference-Guided Fixer for Diffusion-Based View Synthesis

Sihan Chen¹, Xiang Zhang^{†1,2}, Yang Zhang², Tunc Aydin², and
Christopher Schroers²

¹ ETH Zürich, Switzerland

{sihchen, xianzhang}@ethz.ch

² DisneyResearch|Studios, Switzerland

{yang.zhang, tunc.aydin, christopher.schroers}@disneyresearch.com

Abstract. With the recent surge of generative models, diffusion-based approaches have become mainstream for view synthesis tasks, either in an explicit depth-warp-inpaint or in an implicit end-to-end manner. Despite their success, both paradigms often suffer from noticeable quality degradation, *e.g.*, blurred details and distorted structures, caused by pixel-to-latent compression and diffusion hallucination. In this paper, we investigate diffusion degradation from three key dimensions (*i.e.*, spatial, temporal, and backbone-related) and propose **UniFixer**, a universal reference-guided framework that fixes diverse degradation artifacts via a coarse-to-fine strategy. Specifically, a reference pre-alignment module is first designed to perform coarse alignment between the reference view and the degraded novel view. A global structure anchoring mechanism then rectifies geometric distortions to ensure structural fidelity, followed by a local detail injection module that recovers fine-grained texture details for high-quality view synthesis. Our UniFixer serves as a plug-and-play refiner that achieves zero-shot fixing across different types of diffusion degradation, and extensive experiments verify our state-of-the-art performance on novel view synthesis and stereo conversion.

Keywords: Novel view synthesis · Stereo conversion · Diffusion degradation · Plug-and-play enhancement

1 Introduction

View synthesis aims to generate high-fidelity images at novel camera poses, facilitating immersive scene perception beyond the originally captured view-points. Two pivotal tasks have emerged within this domain: Novel View Synthesis (NVS), which renders a scene from previously unseen camera poses [3, 13, 54, 58], and Stereo Conversion (SC), a specialized form of NVS that lifts monocular content to stereoscopic pairs for 3D displays [33, 39, 53, 59]. These capabilities

[†]Corresponding author

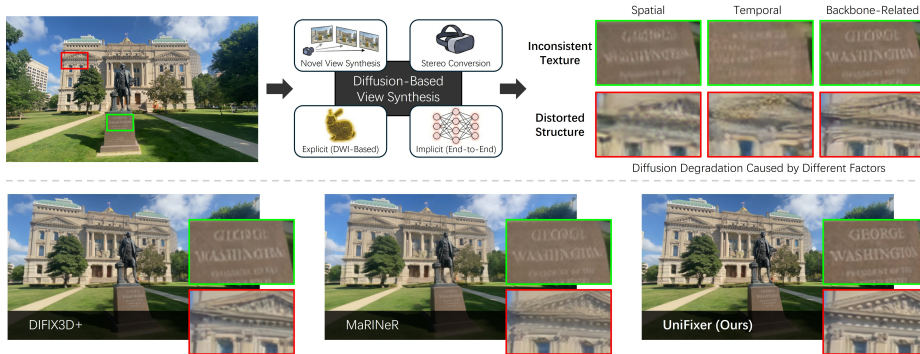


Fig. 1: Existing diffusion-based view synthesis, including explicit/implicit novel view synthesis and stereo conversion approaches, often suffer from diffusion degradations (*e.g.*, inconsistent textures and distorted structures) due to pixel-to-latent compression and diffusion hallucination. Moreover, diffusion degradation varies with different spatial resolutions, temporal dynamics, and diffusion backbones, posing significant challenges for high-fidelity view synthesis. Compared with previous novel view fixers, our UniFixer shows state-of-the-art performance and generalizes to different types of degradations for plug-and-play enhancement.

underpin a wide range of applications, including free-viewpoint video, immersive telepresence, AR/VR, 3D filmmaking, and scalable 3D content creation from casual captures [2, 26, 31].

Recently, diffusion-based generative models have reshaped the landscape of view synthesis. Existing methods typically fall into two paradigms: (i) *explicit Depth-Warp-Inpaint (DWI) methods* that estimate depth, warp observations to the target view, and finally inpaint disoccluded regions [19, 53, 54, 59], and (ii) *implicit end-to-end approaches* that directly generate target views conditioned on the input observations [3, 13, 39]. Despite promising results achieved, both paradigms often produce novel views with degraded structures and texture details (Fig. 1), due to pixel-to-latent compression and diffusion-induced hallucination [33, 57, 58]. Moreover, diffusion degradation varies with multifaceted factors, *e.g.*, spatial resolutions, temporal dynamics, and diffusion backbones, underscoring the pressing demand for a universal and robust novel view fixer.

Several fixers have been developed to improve view synthesis performance by utilizing high-quality reference views [7, 48]. For instance, DIFIX3D+ leverages pre-trained diffusion priors to alleviate artifacts in the rendered novel views [48], and MaRINeR performs deep feature matching to aggregate high-quality features from reference views [7]. However, existing designs primarily operate within low-resolution latent or feature spaces for novel view fixing, which creates an information bottleneck that hinders the transfer of fine-grained textures. Furthermore, previous approaches remain vulnerable to domain shifts and struggle to bridge large viewpoint gaps, often resulting in the loss of high-frequency local details or even the distortions of structures in cases with severe degradation (Fig. 1).

Our goal is to develop a universal novel view fixer that performs robustly across different tasks, model backbones, and degradation patterns without additional re-training. To this end, we present **UniFixer**, a reference-guided framework to fix diverse diffusion degradations in a coarse-to-fine manner. In particular, our UniFixer consists of three main modules: Reference Pre-Alignment (RPA), Global Structure Anchoring (GSA), and Local Detail Injection (LDI). Firstly, we warp the reference view to align with the degraded novel view via RPA, which performs coarse alignment to alleviate the spatial search burden for subsequent feature extraction and correspondence matching. We then employ GSA to aggregate deep features from the reference views and fix structure distortions in the novel views. Finally, we design LDI with deformable convolution and gating mechanisms to adaptively compensate for geometric misalignments and filter out warping artifacts, recovering fine-grained local details for high-fidelity view synthesis. Benefiting from the proposed coarse-to-fine refinement scheme, our UniFixer shows remarkable generalization across different degradation types and achieves state-of-the-art performance when applied to NVS and SC tasks in a plug-and-play manner.

In summary, our main contributions are three-fold:

- We provide a comprehensive analysis of diffusion degradation in view synthesis across three key dimensions: spatial resolution, temporal dynamics, and model architectures. The results show degradation artifacts in even state-of-the-art view synthesis approaches and reveal significant distribution gaps among different degradation types.
- We propose a universal fixer (UniFixer) to handle diverse diffusion degradation in a coarse-to-fine manner. After aligning high-quality reference views via RPA, we employ GSA and LDI modules to progressively correct structure distortions and recover fine-grained texture details for high-quality view synthesis.
- Extensive experiments verify the state-of-the-art performance of our UniFixer in NVS and SC tasks. Furthermore, our method exhibits robust zero-shot generalization to unseen degradation types and functions as a plug-and-play fixer that improves both explicit and implicit view synthesis methods.

2 Related Work

2.1 Explicit View Synthesis

Explicit diffusion-based view synthesis methods typically adopt a Depth-Warp-Inpaint (DWI) pipeline [36, 36, 45, 54, 57, 58]: they first estimate depth/disparity (and camera pose if needed) [21, 27, 50, 56], warp available observations to the target view [34], and then inpaint disoccluded regions using generative diffusion models [19, 20, 54]. Building upon this pipeline, ViewCrafter employs 3D point clouds for novel view rendering and iterative scene reconstruction [54]. GEN3C proposes a 3D-informed video diffusion model to produce consistent novel views

from spatial-temporal 3D caches [36]. Considering that the depth quality is crucial for explicit methods, the recent approach HairGuard designs a depth fixer to improve novel view synthesis quality [58]. For stereo conversion, StereoCrafter proposes an auto-regressive strategy and tiled processing to handle videos with different lengths and resolutions [59], and M2SVid extends the spatial attention in the Stable Video Diffusion [6] for high-quality inpainting [40]. Although DWI-based approaches show advantages in controllability, geometry estimation and warping can be imperfect in practice. For instance, depth/disparity errors and imperfect visibility reasoning often introduce misalignment and distortions near occlusion boundaries and thin structures. Meanwhile, reflective/refractive regions can further make correspondence ambiguous due to multi-depth (non-Lambertian) effects [39].

2.2 Implicit View Synthesis

Implicit view synthesis methods usually perform end-to-end generation without explicit warping or geometry estimation [3, 9, 13, 14, 60]. For instance, ReCamMaster [3] directly synthesizes novel views conditioned on the input observations and camera information (e.g., via Plücker camera embeddings [16, 42]), leveraging diffusion priors for multi-view reasoning and view synthesis. Considering the view-dependent effects and depth ambiguity in complex scenarios, *e.g.*, scenes with transparent objects or reflective surfaces, implicit view synthesis approaches are also employed for stereo conversion [4, 39, 49]. Eye2eye utilizes two diffusion models as a generator and a refiner to produce stereo pairs with realistic view-dependent effects [15]. StereoPilot [39] leverages a pre-trained video diffusion transformer to generate stereoscopic outputs in an end-to-end manner, learning stereo priors from data to address depth ambiguity. While implicit models show promising results under complex scenes and may reduce the dependency on geometry estimators, existing methods often suffer from diffusion degradations, *e.g.*, blurred details and distorted structures, due to pixel-to-latent compression and diffusion-induced hallucination.

2.3 Reference-Guided Fixer

Reference images have been widely used for enhancement in computer vision tasks like super-resolution [5, 8, 29] and style transfer [1, 25, 52]. In view synthesis tasks, a desirable fixer should preserve the overall layout and color distribution while correcting structure distortions and recovering fine-grained details in the novel views. The previous method DIFIX3D+ employs pre-trained diffusion models to aggregate reference features in the latent space for novel view enhancement [48]. However, latent-space fusion can limit the transfer of fine-grained details from the reference image and becomes brittle when large spatial gaps exist between the reference and the degraded view. MaRINeR leverages deep feature matching to estimate the texture correspondence for guided refinement, but the feature matching is often performed on low-resolution feature maps due to computational efficiency, making it difficult to recover fine-grained

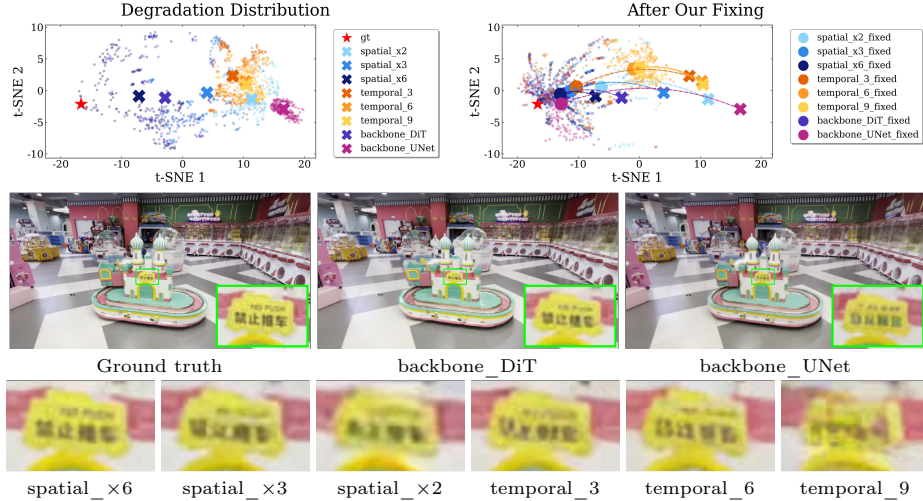


Fig. 2: Degradation analysis with t-SNE feature visualization of spatial ($\times 2 / \times 3 / \times 4 / \times 6$), temporal (frame strides $\in \{1, 3, 6, 9\}$), and backbone-related (UNet [54] and DiT [19]) degradations on a DL3DV [28] scene. The shared setting (spatial $\times 4$, temporal stride 1, and DiT-based backbone) is plotted once as backbone_DiT. Color families denote degradation types, and the red star marks the ground-truth. Crosses/circles denote cluster means before/after our fixing for each degradation type, with dashed arrows indicating the shift. Each cluster comprises 250 samples, with outliers beyond 1σ omitted for clarity. Visual examples of different diffusion degradations are provided.

textures [7]. In contrast, our UniFixer designs a coarse-to-fine pipeline to improve both global structures and local texture details for high-fidelity view synthesis.

3 Degradation Analysis

Due to pixel-to-latent compression and diffusion hallucination, existing diffusion-based view synthesis methods often suffer from degradations like distorted structures and inconsistent textures, as illustrated in Fig. 1. To facilitate the analysis of diffusion degradations, we first introduce a feature visualization approach using t-SNE [30]. Given a degraded image I_{deg} , *i.e.*, outputs from diffusion-based view synthesis methods, and its corresponding ground truth I_{gt} , we extract per-image features F_{deg} and F_{gt} using a frozen DINOv3 [41] encoder $\Phi(\cdot)$, *i.e.*,

$$F_{deg} = \Phi(I_{deg}) \in \mathbb{R}^{L \times D}, F_{gt} = \Phi(I_{gt}) \in \mathbb{R}^{L \times D}, \quad (1)$$

where L and D indicate the number and dimension of tokens. We only keep patch tokens in F_{deg} and F_{gt} to focus on local degradation details. Then, we aggregate patch tokens into compact per-image embeddings by concatenating the mean and standard deviation over all patch tokens, *i.e.*, $\hat{F}_i = [\mu(F_i), \sigma(F_i)] \in \mathbb{R}^{2D}$, $i \in \{deg, gt\}$, where $[\cdot, \cdot]$ denotes concatenation. Finally, we compute the difference

between \hat{F}_{deg} and \hat{F}_{gt} as the feature representation of diffusion degradations, *i.e.*,

$$\hat{F}_{diff} = |\hat{F}_{deg} - \hat{F}_{gt}| \in \mathbb{R}^{2D}. \quad (2)$$

Eq. (2) mitigates the impact of the image content in the feature representation to facilitate the analysis of diffusion degradations.

Leveraging the feature visualization protocol, we investigate diffusion degradations from three key dimensions: spatial resolutions, temporal dynamics, and diffusion backbones:

- **Spatial Degradation.** Spatial degradation is one of the most common degradation types for diffusion-based models. Since modern diffusion models typically project images into the latent space to alleviate computational overhead via a Variational Auto-Encoder (VAE) [24], the latent spatial resolution directly affects the synthesis fidelity. Following [41], we keep the VAE compression ratio fixed and draw the feature distributions under varying input image resolutions (*i.e.*, 240×416 / 360×624 / 480×832 / 720×1248 , denoted by $\times 2/$ $\times 3/$ $\times 4/$ $\times 6$ in Fig. 2). Due to the pixel-to-latent compression, latents with lower resolution inevitably attenuate high-frequency textures and sharp edges, leading to over-smoothed details (Fig. 2). While scaling up the input resolution preserves finer spatial details at the expense of increased computational cost, diffusion artifacts, *e.g.*, hallucination, persist in the synthesized views due to the generative nature of diffusion models.
- **Temporal Degradation.** Recent diffusion models design spatio-temporal VAEs and temporal attention mechanisms to model temporal dynamics and enforce inter-frame coherence [6, 43]. However, these methods often struggle under rapid camera motions. Specifically, inter-frame correspondences weaken significantly under large viewpoint shifts, causing temporal priors to either over-smooth high-frequency textures or hallucinate inconsistent details (Fig. 2). To investigate this, we simulate varying degrees of camera motion by modulating the temporal stride between sampled frames (*i.e.*, frame stride $\in \{1, 3, 6, 9\}$). Larger intervals yield more significant camera spatial displacements, thereby exacerbating the severity of temporal degradation.
- **Backbone-related Degradation.** Finally, we investigate backbone-specific degradations by comparing the two predominant generative architectures: convolutional UNets [37] and transformer-based models (DiTs) [35]. Despite both operating within similar latent diffusion paradigms, their distinct inductive biases result in different artifact distributions (Fig. 2). Specifically, convolution-based UNets tend to over-smooth fine textures after repeated down-/up-sampling. Although DiT-based models exhibit superior performance over UNet-based ones, transformer backbones often introduce patch-wise inconsistencies or structure hallucinations under strong domain shifts.

As shown in Fig. 2, degradations from different dimensions form separated distributions in the feature space, with varying scales inducing further distributional shifts. Despite the distributional divergence across degradation types and scales, our UniFixer consistently pushes each degradation cluster towards

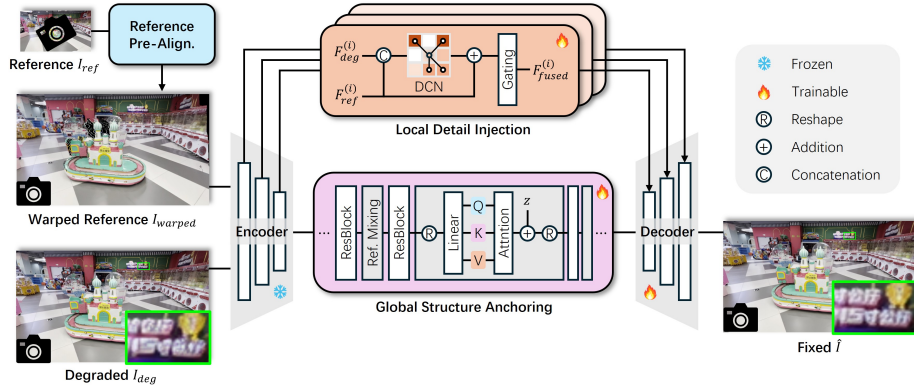


Fig. 3: Pipeline of UniFixer. Given a degraded novel view and a high-quality reference view, we first perform coarse alignment by the reference pre-alignment module. Leveraging the warped reference, we apply the global structure anchoring module to aggregate shared structures via reference-mixed attention. The local detail injection module adaptively fuses multi-scale features for fine-grained texture enhancement.

the ground-truth, demonstrating robust zero-shot generalization across diverse diffusion degradations.

4 Method

Given a degraded novel view $I_{deg} \in \mathbb{R}^{3 \times H \times W}$ from view synthesis methods (*e.g.*, NVS or SC) and a reference image $I_{ref} \in \mathbb{R}^{3 \times H \times W}$, our goal is to reconstruct a high-quality image $\hat{I} \in \mathbb{R}^{3 \times H \times W}$ that corrects distorted structures and restores texture details in the novel view. To handle diverse diffusion degradations with a universal fixer, we design a coarse-to-fine refinement framework as shown in Fig. 3. Specifically, we first perform reference pre-alignment (Sec. 4.1) to warp reference images toward the target novel view, thereby reducing the spatial search space for subsequent feature extraction and correspondence matching. With the pre-aligned reference, we anchor shared structural information in deep features via reference-mixed self-attention (Sec. 4.2). To recover fine-grained texture details, we design local detail injection modules to adaptively fuse reference features for enhancement while filtering warping errors (Sec. 4.3). Finally, an efficient strategy is proposed for model training (Sec. 4.4).

4.1 Reference Pre-Alignment

To alleviate the difficulty of long-range correspondence search, we first perform coarse alignment by warping I_{ref} to the camera view of I_{deg} , generating the warped reference I_{warped} . This step brings relevant structural cues directly into the local spatial neighborhood of each pixel in I_{deg} , transforming an exhaustive global correspondence search into a tractable, localized refinement task.

Furthermore, by operating directly in the raw pixel space, this warping process preserves fine-grained texture details that are crucial for high-fidelity view synthesis. Specifically, the pre-alignment process can be formulated as

$$I_{warped} = \mathcal{W}(I_{ref}, T), \quad (3)$$

where $\mathcal{W}(\cdot)$ denotes the warping operator (*e.g.*, softmax splatting [34]), and T indicates the view transformation map.

As shown in Fig. 4, the generation of I_{warped} depends on the type of view synthesis approaches:

- **Geometry-Based Warping for Explicit Methods:** For methods following the Depth-Warp-Inpaint (DWI) paradigm, the warped reference I_{warped} is usually accessible through geometric transformations. Depending on the view synthesis task, this is typically achieved via perspective projection for NVS or disparity mapping for SC. Aligning with these established pipelines, we employ geometry-based warping to perform pre-alignment.
- **Flow-Based Warping for Implicit Methods:** Implicit view synthesis approaches usually render novel views in an end-to-end manner without relying on explicit geometry like depth maps [3, 39], making geometry-based warping difficult. Nevertheless, recent implicit view synthesis methods have exhibited promising performance in achieving the overall appearance consistency across view-points, *e.g.*, layout, illumination, and color distribution. Leveraging this characteristic, we perform flow-based warping with the optical flow estimated from the reference and the synthesized view (SEA-RAFT [46] is used in our implementation) for reference pre-alignment.

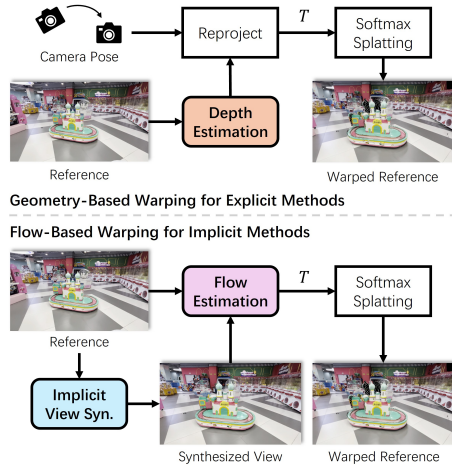


Fig. 4: Reference pre-alignment. For explicit view synthesis methods, *i.e.*, DWI-based methods, we estimate depth information and perform geometry-based warping using camera poses. For implicit approaches, we perform flow-based warping with the optical flow estimated from the reference and the synthesized novel view.

4.2 Global Structure Anchoring

The goal of GSA is to leverage deep features from the reference view to rectify structural distortions, while simultaneously preserving the high-level semantics (such as the overall layout and appearance) of the degraded view. To

this end, we implement UniFixer upon the pre-trained one-step diffusion model, SD-Turbo [38], to harness the robust feature extraction capabilities learned by its attention layers. To efficiently aggregate reference features, we follow DIFIX3D+ [48] to implement the reference mixing mechanism in self-attention layers. Specifically, we first extract the latent space representations of I_{deg} and I_{warped} , and concatenate them as input to GSA, denoted by \mathbf{z} :

$$\mathbf{z} = [\mathcal{E}(I_{deg}), \mathcal{E}(I_{warped})] \in \mathbb{R}^{2C \times H \times W} \quad (4)$$

where $\mathcal{E}(\cdot)$ denotes the frozen latent encoder. To capture the structural information in the reference view, we reshape the latents into a token sequence $\mathbf{z} \in \mathbb{R}^{(2HW) \times C}$. The anchoring operation is then defined as:

$$\mathbf{z} := \mathbf{z} + \text{Softmax} \left(\frac{QK^T}{\sqrt{d}} \right) V, \quad Q, K, V = \text{Linear}(\mathbf{z}). \quad (5)$$

By computing attention across the concatenated $2 \times H \times W$ spatial-view tokens and applying a residual connection to the base latent representation, the features of I_{deg} serve as anchors to aggregate shared structures from the reference view. Consequently, this process enforces structural alignment and regularizes the diffusion process to prevent content and color drift.

4.3 Local Detail Injection

Restoring high-fidelity textures requires fine-grained spatial cues. However, the spatial compression inherent in the pixel-to-latent conversion often fails to preserve high-frequency details in the bottleneck latent \mathbf{z} , making the recovery of high-fidelity textures highly ill-posed. To this end, we propose the LDI module to adaptively fuse fine-grained features from the latent encoder for local detail refinement.

The LDI operates across multiple feature scales. For each scale i , we extract the intermediate feature maps from the frozen encoder \mathcal{E} , *i.e.*,

$$\left(F_{deg}^{(i)} \right)_{i=1}^n \leftarrow \mathcal{E}(I_{deg}), \quad \left(F_{ref}^{(i)} \right)_{i=1}^n \leftarrow \mathcal{E}(I_{warped}), \quad (6)$$

where $F^{(i)} \in \mathbb{R}^{C_i \times H_i \times W_i}$ denotes the feature at the i -th feature scale, and n indicates the total number of feature scales. As these features are extracted before the deep bottleneck, they preserve rich low-level geometric cues and fine-grained texture information. However, since the coarse alignment in RPA (Sec. 4.1) often suffers from inaccuracies, either originating from depth estimation errors or from noisy optical flow, directly fusing these encoder features would introduce ghosting artifacts and blurriness. To address this, we perform detail injection through adaptive warping deformation and uncertainty-aware gated fusion.

Adaptive Warping Deformation. For each scale i , we employ Deformable Convolutional Networks (DCN) [10] to rectify micro-misalignments. Since I_{warped} is already in the spatial neighborhood of I_{deg} , the DCN only needs to predict

small-range offsets $\Delta p^{(i)}$ and the associated mask $M^{(i)}$ to establish precise correspondence, *i.e.*,

$$(\Delta p^{(i)}, M^{(i)}) = \mathcal{P}_\theta^{(i)}([F_{deg}^{(i)}, F_{ref}^{(i)}]), \quad (7)$$

$$\tilde{F}_{ref}^{(i)} = F_{ref}^{(i)} + \text{DCN}(F_{ref}^{(i)}, \Delta p^{(i)}, M^{(i)}), \quad (8)$$

where $\mathcal{P}_\theta^{(i)}$ denotes the offset and mask estimator of the i -th scale. By deforming the reference features, high-frequency details from the warped reference are accurately aligned to enhance the degraded view.

Uncertainty-Aware Gated Fusion. Despite the adaptive deformation of DCN, certain regions (*e.g.*, occlusions or areas with extreme distortion) in $\tilde{F}_{ref}^{(i)}$ may remain unreliable due to warping errors. To prevent these artifacts from propagating through the restoration pipeline, we introduce a gated fusion mechanism to estimate the confidence of the reference cues:

$$G^{(i)} = \sigma\left(\text{Conv}\left([F_{deg}^{(i)}, \tilde{F}_{ref}^{(i)}]\right)\right), \quad (9)$$

$$F_{fused}^{(i)} = G^{(i)} \odot F_{deg}^{(i)} + (1 - G^{(i)}) \odot \tilde{F}_{ref}^{(i)}, \quad (10)$$

where $\text{Conv}(\cdot)$ is 2D convolution layer, σ is the Sigmoid function, \odot is the element-wise multiplication, and $G^{(i)} \in [0, 1]^{C_i \times H_i \times W_i}$ is the estimated confidence map. This adaptive fusion allows the fixer to select high-fidelity features from $\tilde{F}_{ref}^{(i)}$ while filtering artifacts caused by warping errors. Finally, the fused feature $F_{fused}^{(i)}$ is injected into the corresponding decoder layer to guide the decoding of \mathbf{z} , *i.e.*,

$$\hat{I} = \mathcal{D}(\mathbf{z}, \mathbf{f}), \quad (11)$$

where $\mathcal{D}(\cdot)$ denotes the latent decoder, and $\mathbf{f} = (F_{fused}^{(i)})_{i=1}^n$.

4.4 Model Training

We propose a simple strategy to curate paired data $\{(I_{deg}^{(i)}, I_{warped}^{(i)}, I_{gt}^{(i)})\}_i$ for model training, where $I_{gt}^{(i)}$ indicates the ground-truth image. Given an image sequence $(I_{gt}^{(i)})_{i=1}^N$ from the training dataset with N denoting the sequence length, we first estimate the scene geometry, *e.g.*, depth and camera poses, via scene reconstruction methods (DA3 [27] is used in our implementation). Then, we select the middle frame as the reference image $I_{ref} := I_{gt}^{(\lceil N/2 \rceil)}$ and generate the warped references $(I_{warped}^{(i)})_{i=1}^N$ by warping I_{ref} to the other viewpoints (note that $I_{warped}^{(\lceil N/2 \rceil)} := I_{ref}$ at the reference viewpoint). Following that, we synthesize the degraded images $(I_{deg}^{(i)})_{i=1}^N$ by applying diffusion models (VACE [19] is used in UniFixer) to re-generate the ground-truth images $(I_{gt}^{(i)})_{i=1}^N$, *i.e.*,

$$(I_{deg}^{(i)})_{i=1}^N = \text{Diffusion}\left(\left(I_{gt}^{(i)}\right)_{i=1}^N\right). \quad (12)$$

Consequently, we synthesize $(I_{deg}^{(i)})_{i=1}^N$ with diffusion degradations while ensuring that the underlying scene content remains semantically consistent with $(I_{gt}^{(i)})_{i=1}^N$. This design encourages the model to preserve the overall scene content, *e.g.*, layout and appearance, of the novel view while fixing diffusion degradation artifacts. Finally, we train UniFixer using ℓ_2 loss \mathcal{L}_2 and perceptual loss \mathcal{L}_{lpiPs} [55]:

$$\mathcal{L} = \mathcal{L}_2(\hat{I}, I_{gt}) + \lambda_{lpiPs} \cdot \mathcal{L}_{lpiPs}(\hat{I}, I_{gt}), \quad (13)$$

where λ_{lpiPs} indicates the balancing weight.

Although diffusion degradation varies with different factors, *e.g.*, spatial resolutions, temporal dynamics, and diffusion backbones (Sec. 3), our training is performed under a fixed configuration (*i.e.*, constant resolution, fixed motion speed, and a single diffusion backbone). By leveraging the coarse-to-fine alignment framework, we shift the learning objective from the degradation-specific modeling to local correspondence searching and reference aggregation. This design bypasses the challenge of explicitly modeling distribution shifts across diverse diffusion degradations, enabling robust zero-shot generalization without the need for extensive retraining or fine-tuning.

5 Experiment and Analysis

5.1 Experimental Settings

Training. Our training set is curated from the first 1K scenes of the DL3DV dataset [28], which we empirically find to be sufficient for achieving state-of-the-art performance. UniFixer is optimized using Adam [23] with a learning rate of 2×10^{-5} and a batch size of 1 on 480×832 patches, with $\lambda_{lpiPs} = 1.0$. The training process converges within 50K iterations, requiring approximately 14 hours on a single NVIDIA A100 GPU (40GB).

Evaluation. We employ the DL3DV test benchmark [28], Mono2Stereo dataset [53], Spring dataset [32], and the Spatial Video Dataset (SVD) [18] for evaluation. For explicit view synthesis methods, we report PSNR, SSIM [47], LPIPS [55], DISTS [11], and FID [17]. For implicit approaches, where the synthesized outputs may deviate spatially from the ground truth, we use non-reference metrics, including CLIP-IQA [44], MUSIQ [22], and MANIQA [51]. FID is also computed between the fixed results and the source video frames to measure distribution differences. We mainly compare UniFixer with state-of-the-art novel view fixers DIFIX3D+ [48] and MaRINeR [7]. To ensure fair comparisons, we retrain DIFIX3D+ and MaRINeR on our training dataset using their official training codes. For degradation analysis and ablation study, we conduct our experiments under the NVS setting.

5.2 Degradation Fixing

Following the same experimental setting in Sec. 3 and Fig. 2, we evaluate the degradation fixing performance of UniFixer across three prevalent degradation

Table 1: Degradation fixing for novel view synthesis on the DL3DV dataset. Spatial, temporal, and backbone-related degradation denotes degradation from different input resolutions, camera motion speeds, and diffusion backbones, respectively (Sec. 3). **Best** results are marked.

Degradation	Fixer	PSNR \uparrow	SSIM \uparrow	LPIPS \downarrow	DISTS \downarrow	FID \downarrow	PSNR \uparrow	SSIM \uparrow	LPIPS \downarrow	DISTS \downarrow	FID \downarrow	
Spatial		$\times 2$ (240 \times 416)					$\times 3$ (360 \times 624)					
	W/O fixer	21.35	0.680	0.309	0.183	37.16	22.72	0.727	0.227	0.135	23.41	
	DIFIX3D+ [48]	21.60	0.692	0.275	0.148	31.11	22.86	0.732	0.195	0.103	20.81	
	MaRINeR [7]	21.67	0.706	0.238	0.140	33.73	23.08	0.750	0.179	0.103	22.69	
	Ours	22.10	0.754	0.232	0.127	26.55	23.37	0.784	0.164	0.088	18.27	
		$\times 4$ (480 \times 832)					$\times 6$ (720 \times 1248)					
	W/O fixer	23.43	0.750	0.175	0.105	19.96	24.01	0.777	0.179	0.107	17.45	
	DIFIX3D+ [48]	23.53	0.752	0.158	0.082	18.27	23.48	0.762	0.174	0.088	17.87	
	MaRINeR [7]	23.75	0.769	0.157	0.089	19.94	23.61	0.772	0.157	0.087	18.84	
	Ours	24.03	0.793	0.138	0.072	16.66	24.32	0.798	0.142	0.074	15.69	
	Temporal		Stride=1					Stride=3				
		W/O fixer	23.43	0.750	0.175	0.105	19.96	19.89	0.620	0.318	0.194	41.94
DIFIX3D+ [48]		23.53	0.752	0.158	0.082	18.27	20.00	0.626	0.289	0.156	33.55	
MaRINeR [7]		23.75	0.769	0.157	0.089	19.94	20.05	0.635	0.310	0.186	41.39	
Ours		24.03	0.793	0.138	0.072	16.66	20.23	0.656	0.276	0.150	33.01	
		Stride=6					Stride=9					
W/O fixer		18.83	0.594	0.389	0.238	56.09	18.16	0.585	0.435	0.264	66.09	
DIFIX3D+ [48]		18.98	0.604	0.355	0.200	43.69	18.30	0.595	0.402	0.228	51.81	
MaRINeR [7]		18.94	0.610	0.378	0.231	53.66	18.22	0.599	0.425	0.258	62.95	
Ours		19.23	0.644	0.334	0.190	42.49	18.54	0.636	0.380	0.218	50.24	
Backbone			UNet					DiT				
		W/O fixer	21.45	0.669	0.194	0.102	22.85	23.43	0.750	0.175	0.105	19.96
	DIFIX3D+ [48]	21.38	0.666	0.182	0.095	23.90	23.53	0.752	0.158	0.082	18.27	
	MaRINeR [7]	21.48	0.670	0.187	0.094	22.54	23.75	0.769	0.157	0.089	19.94	
	Ours	22.19	0.739	0.170	0.086	20.84	24.03	0.793	0.138	0.072	16.66	

types in diffusion-based view synthesis, including spatial, temporal, and backbone-related degradations. Although our method is trained under a fixed configuration (*i.e.*, spatial resolution 480 \times 832, temporal stride equal to 1, and DiT-based backbone), UniFixer achieves state-of-the-art performance and shows strong zero-shot generalization across different degradation types and difficulty levels, as shown in Tab. 1.

5.3 View Synthesis Fixing

We evaluate the performance of UniFixer on the NVS and SC tasks. As shown in Fig. 12, our method outperforms previous novel view fixers in recovering fine-grained structure and texture details. In the SC task, we employ the recent Mono2Stereo [53] and StereoCrafter [59] to generate right views from left-view inputs, and UniFixer achieves significant improvements in the perceptual quality of novel views, as shown in Fig. 12 and Tab. 2. We also apply UniFixer to enhance implicit view synthesis approaches (*i.e.*, ReCamMaster [3] for NVS and StereoPilot [39] for SC) in a plug-and-play manner, and our proposed method consistently shows superior results over existing novel view fixers (Tab. 3).

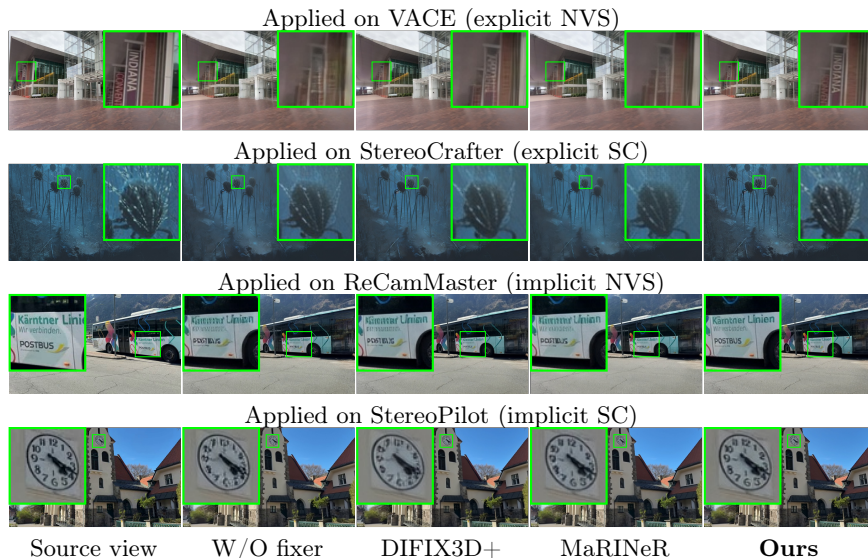


Fig. 5: Visual results of applying novel view fixers (including DIFIX3D+ [48], MaRINeR [7], and ours) to improve diffusion-based view synthesis methods.

5.4 Ablation Study

Component design. Tab. 5 demonstrates the contributions of each component in our UniFixer pipeline. Compared with the variant that directly utilizes features from the reference view (#1), RPA alleviates the difficulty of correspondence search via pre-alignment, yielding significant performance improvement (#2 *vs.* #1). GSA aggregates the shared structures between reference and target views, providing a crucial foundation for degradation removal (#4 *vs.* #3). Finally, incorporating the LDI module enables the adaptive extraction of high-fidelity reference details while suppressing warping artifacts (#4 *vs.* #2).

Referencing mechanism. Many referencing mechanisms have been designed to leverage reference features for enhancement. We compare our warping-based referencing method against three representative paradigms: skip connection (convolution-based) [48], cross attention (attention-based) [12], and feature matching (matching-based) [7]. For fair comparisons, we use the same backbone (SD-Turbo [38]) and replace our RPA and LDI modules with different referencing mechanisms. All variants are trained under the same setting. The proposed warping-based referencing facilitates the recovery of fine-grained structures and textures (see supp. for the visual comparisons), and Tab. 4b verifies our superior performance over previous referencing methods.

Table 2: Stereo conversion on Mono2Stereo [53] and Spring [32] datasets. We perform stereo conversion using the state-of-the-art methods Mono2Stereo [53] and StereoCrafter [59]. **Best** results are marked.

Dataset	Fixer	Mono2Stereo [53] output					StereoCrafter [59] output				
		PSNR \uparrow	SSIM \uparrow	LPIPS \downarrow	DISTS \downarrow	FID \downarrow	PSNR \uparrow	SSIM \uparrow	LPIPS \downarrow	DISTS \downarrow	FID \downarrow
Mono2Stereo [53]	W/O fixer	29.52	0.847	0.101	0.071	10.66	30.33	0.893	0.108	0.086	14.68
	DIFIX3D+ [48]	29.20	0.852	0.098	0.071	9.90	30.31	0.896	0.106	0.087	13.82
	MaRINeR [7]	29.91	0.861	0.115	0.081	12.12	30.61	0.903	0.107	0.086	14.66
	Ours	30.01	0.882	0.088	0.065	9.29	30.84	0.916	0.087	0.073	10.50
Spring [32]	W/O fixer	27.43	0.645	0.167	0.092	34.53	26.82	0.702	0.257	0.153	91.87
	DIFIX3D+ [48]	27.46	0.654	0.174	0.102	32.64	26.64	0.706	0.240	0.145	72.77
	MaRINeR [7]	27.66	0.661	0.216	0.134	41.28	26.87	0.703	0.303	0.179	89.25
	Ours	29.35	0.827	0.127	0.086	29.43	28.04	0.843	0.167	0.113	47.22

Table 3: Implicit view synthesis on the Spring [32] and SVD [18] datasets. We employ the state-of-the-art implicit methods for view synthesis (ReCamMaster [3] for NVS and StereoPilot [39] for SC). **Best** results are marked.

Dataset	Method	ReCamMaster [3] output				StereoPilot [39] output			
		CLIP-IQA \uparrow	MUSIQ \uparrow	MANIQA \uparrow	FID \downarrow	CLIP-IQA \uparrow	MUSIQ \uparrow	MANIQA \uparrow	FID \downarrow
Spring [32]	W/O fixer	0.347	54.38	0.272	72.21	0.344	49.79	0.331	90.44
	DIFIX3D+ [48]	0.453	54.26	0.260	76.88	0.389	48.77	0.311	94.15
	MaRINeR [7]	0.429	53.13	0.276	73.38	0.378	48.41	0.296	83.93
	Ours	0.482	55.75	0.282	70.12	0.452	50.62	0.319	77.67
SVD [18]	W/O fixer	0.417	71.72	0.396	23.69	0.405	71.67	0.442	25.18
	DIFIX3D+ [48]	0.494	70.99	0.372	24.57	0.484	70.08	0.397	24.82
	MaRINeR [7]	0.524	71.19	0.392	23.53	0.525	70.89	0.411	19.30
	Ours	0.531	72.00	0.410	22.36	0.538	71.67	0.436	18.42

Table 4: Ablation study on (a) component designs and (b) referencing mechanisms.

(a) Component design ablation.

ID	Components			Metrics				
	GSA	RPA	LDI	PSNR \uparrow	SSIM \uparrow	LPIPS \downarrow	DISTS \downarrow	FID \downarrow
#1	✓			26.19	0.812	0.113	0.066	24.23
#2	✓	✓		27.09	0.866	0.092	0.055	20.62
#3	✓	✓	✓	25.86	0.859	0.114	0.068	24.95
#4	✓	✓	✓	27.37	0.875	0.084	0.051	20.05

(b) Referencing mechanism ablation.

ID	Type	Method	PSNR \uparrow	SSIM \uparrow	LPIPS \downarrow	DISTS \downarrow	FID \downarrow
#1	Convolution	Skip connection [48]	26.19	0.812	0.113	0.066	24.23
#2	Attention	Cross attention [12]	25.87	0.798	0.118	0.070	26.89
#3	Matching	Feature matching [7]	26.14	0.811	0.106	0.060	24.54
#4	Warping	Ours	27.37	0.875	0.084	0.051	20.05

6 Conclusion

In this paper, we systematically analyze three prevalent degradation types in diffusion-based view synthesis and propose a universal reference-guided framework to address them in a coarse-to-fine manner. We first perform reference pre-alignment to facilitate correspondence search, then aggregate deep features for global structure anchoring, and finally inject fine-grained texture details to achieve high-quality view synthesis. Extensive experiments demonstrate the state-of-the-art performance of UniFixer in NVS and SC tasks and verify our zero-shot generalization across different diffusion degradations.

Supplementary Material

Overview

This supplementary material provides additional details that complement the main paper, including more ablation experiments, degradation analysis details, limitation analysis, discussion and visual results.

7 Ablation study details

7.1 More ablation on local detail injection

Table 5: Ablation study on component designs in the proposed LDI module.

ID	Components		Metrics				
	AWD	UAGF	PSNR \uparrow	SSIM \uparrow	LPIPS \downarrow	DISTS \downarrow	FID \downarrow
#1			27.09	0.866	0.092	0.055	20.62
#2	✓		27.18	0.870	0.089	0.053	20.83
#3	✓	✓	27.37	0.875	0.084	0.051	20.05

Our Local Detail Injection (LDI) module consists of two key designs: (i) *Adaptive Warping Deformation* (AWD) for better local alignment, and (ii) *Uncertainty-Aware Gated Fusion* (UAGF) for selectively injecting reliable reference details. While the main paper ablates LDI as a whole module, here we further disentangle LDI and study the contribution of each design by progressively enabling AWD and UAGF, as summarized in Table 5. Specifically, #1 removes both component, #2 enables AWD only, #3 enables both components. Both AWD and UAGF consistently contribute to LDI, and combining them yields the best performance, validating the effectiveness of each design.

7.2 Visual results on ablation study

To complement the quantitative results reported in Tab. 4 of the main paper, we provide additional visual comparisons for the ablation study (Fig. 6). For component design ablation, our RPA makes the correspondence search easier (#2 vs. #1 in Tab. 4a), LDI leads to more fine-grained details recovering (#4 vs. #2 in Tab. 4a), and GSA contributes to better global structure anchoring (#4 vs. #3 in Tab. 4a). For the referencing mechanism ablation, our warping-based referencing restores the finest details among all variants (#4 in Tab. 4b).

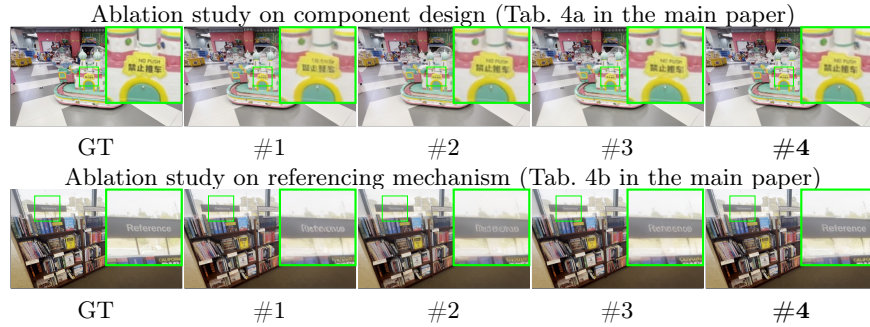


Fig. 6: Visual results of ablation study on component design and referencing mechanism, respectively. The ID corresponds to the ID in Tab. 4a and 4b of the main paper.

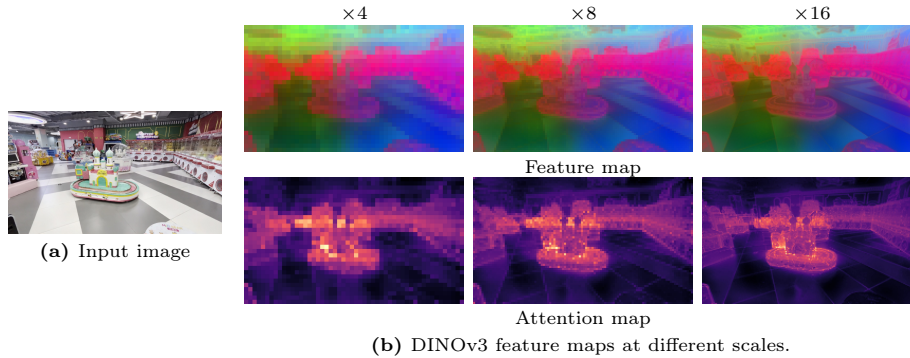


Fig. 7: DINOv3 feature map visualization.

8 Degradation analysis details

8.1 DINOv3 map visualization

To further justify using DINOv3 patch tokens to extract degradation features for the t-SNE analysis, we visualize the token representations of a single degraded image. Specifically, we feed the same image at three input resolutions (*i.e.*, 480×832 / 960×1664 / 1920×3328 , denoted by $\times 4 / \times 8 / \times 16$ in Fig. 7). We then (1) reshape the patch tokens back to a spatial grid and apply PCA to project the features to 3 dimensions for RGB rendering, producing the *feature maps*; and (2) use the CLS token to compute attention scores over patch tokens and visualize them as a heatmap, producing the *attention maps*. Finally, for fair comparison across input resolutions, we resize all visualizations to a standard resolution of 480×832 . From the visualizations, we observe that the feature maps from patch tokens preserve rich fine-grained details, indicating that they are well suited for deriving degradation features in our subsequent analysis. Meanwhile, the attention maps between the CLS token and patch tokens highlight

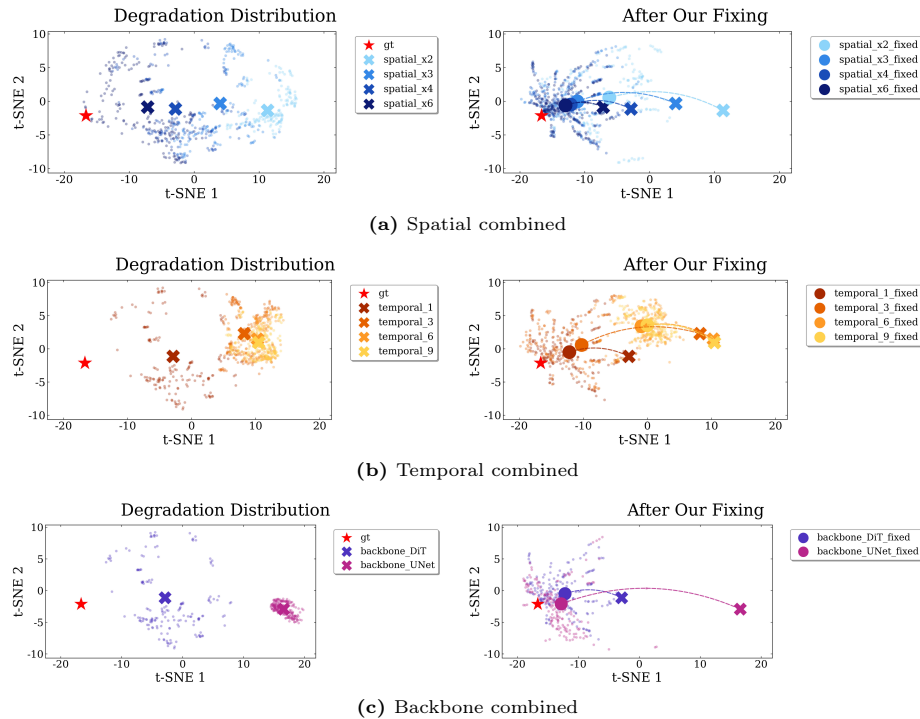


Fig. 8: t-SNE visualization under different degradation dimensions. Lighter colors indicate more severe degradation.

semantically related regions, further supporting the semantic consistency and representational validity of the patch tokens.

8.2 Degradation fixing results

We further split the all-in-one t-SNE figure (Fig. 2 in the main paper) into three subfigures corresponding to different degradation dimensions (*i.e.*, spatial, temporal, and backbone-related) in Fig. 8. We also provide the corresponding degradation and fixed visual results in Fig. 9, where the visual quality consistently improves as the degradation severity decreases (across rows) and as more effective fixing methods are applied (across columns). These results are a subset of the samples used to produce the t-SNE visualization.

9 Limitation analysis

For implicit end-to-end approaches, we estimate the optical flow via SEA-RAFT [46] between the diffusion-synthesized target image and the source image; however,

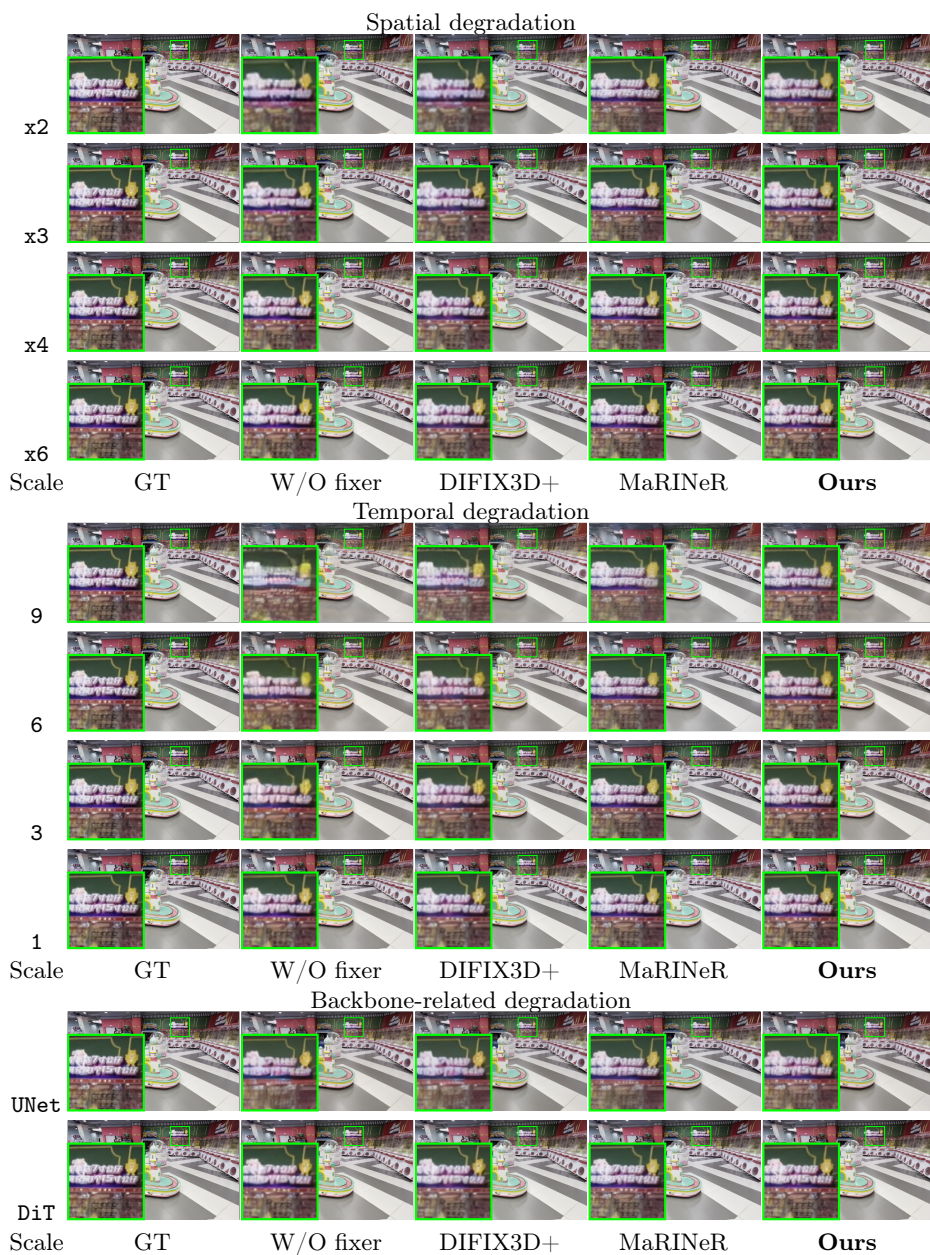


Fig. 9: Additional degradation and fixing visual results. The visual quality consistently improves as the degradation severity decreases (across rows) and as more effective fixers are applied (across columns). These results are a subset of the samples used to produce the t-SNE visualization.

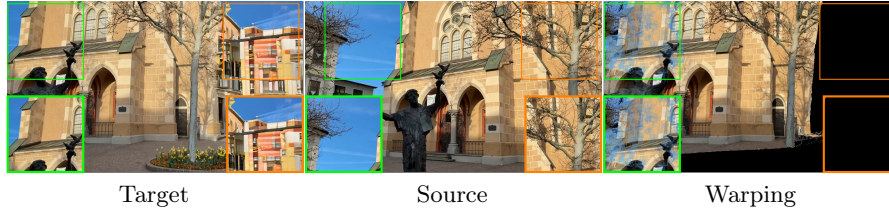


Fig. 10: Flow-based warping failure case.

when the viewpoint change between target and source view is large, SEA-RAFT can struggle to estimate accurate correspondences, which further leads to erroneous warping (Fig. 10).

10 Discussion

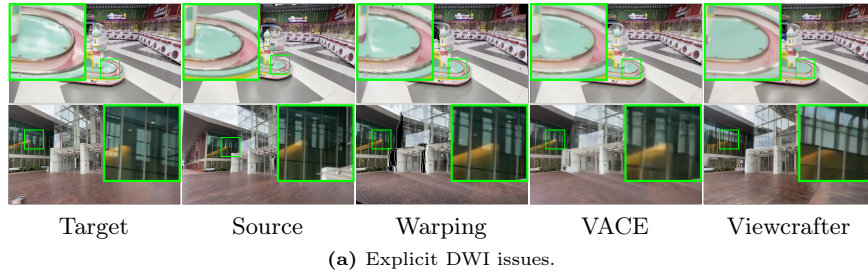


Fig. 11: Warping and view-dependent effects discussion.

For explicit DWI methods, we observe two main issues: (1) view-dependent effects can be baked into the estimated geometry and thus propagated by warping; (2) a single surface point is typically constrained to have a single depth, which cannot represent multi-depth structures (e.g., semi-transparent or layered regions), leading to warping errors. These errors are then propagated to

the inpainting stage, often leading DWI methods to produce corrupted or unreal outputs (Fig. 11a). However, for the case that upstream models already generate possible view-dependent effects (VDE), although our UniFixer relies on RPA, the proposed UAGF enables us to preserve such VDE when the warped regions are assessed to be *unreliable*, instead of blindly overwriting them using warping during fixing (Fig. 11b).

11 More visual results

11.1 Benchmark fixing results

We evaluate our method on six upstream baseline models in total for both NVS and SC tasks (*i.e.*, VACE [19], ViewCrafter [54], Mono2Stereo [53], StereoCrafter [59], RecamMaster [3], and StereoPilot [39]) on DL3DV [28], Spring [32], Mono2stereo [53] and Spatial Video Dataset [18]. As shown in Fig. 12, our approach consistently fixed the view synthesis degradation in the outputs of the upstream models and outperforms state-of-the-art novel view fixers (*i.e.*, DIFIX3D+ [48] and MaRINeR [7]).

11.2 In-the-wild fixing results

We perform more in-the-wild tests. Specifically, we use VACE [19], serving as the representative example of explicit DWI pipeline. By simply applying our plug-and-play fixer, we can significantly remove the degradation and improve the visual quality (Fig. 13).

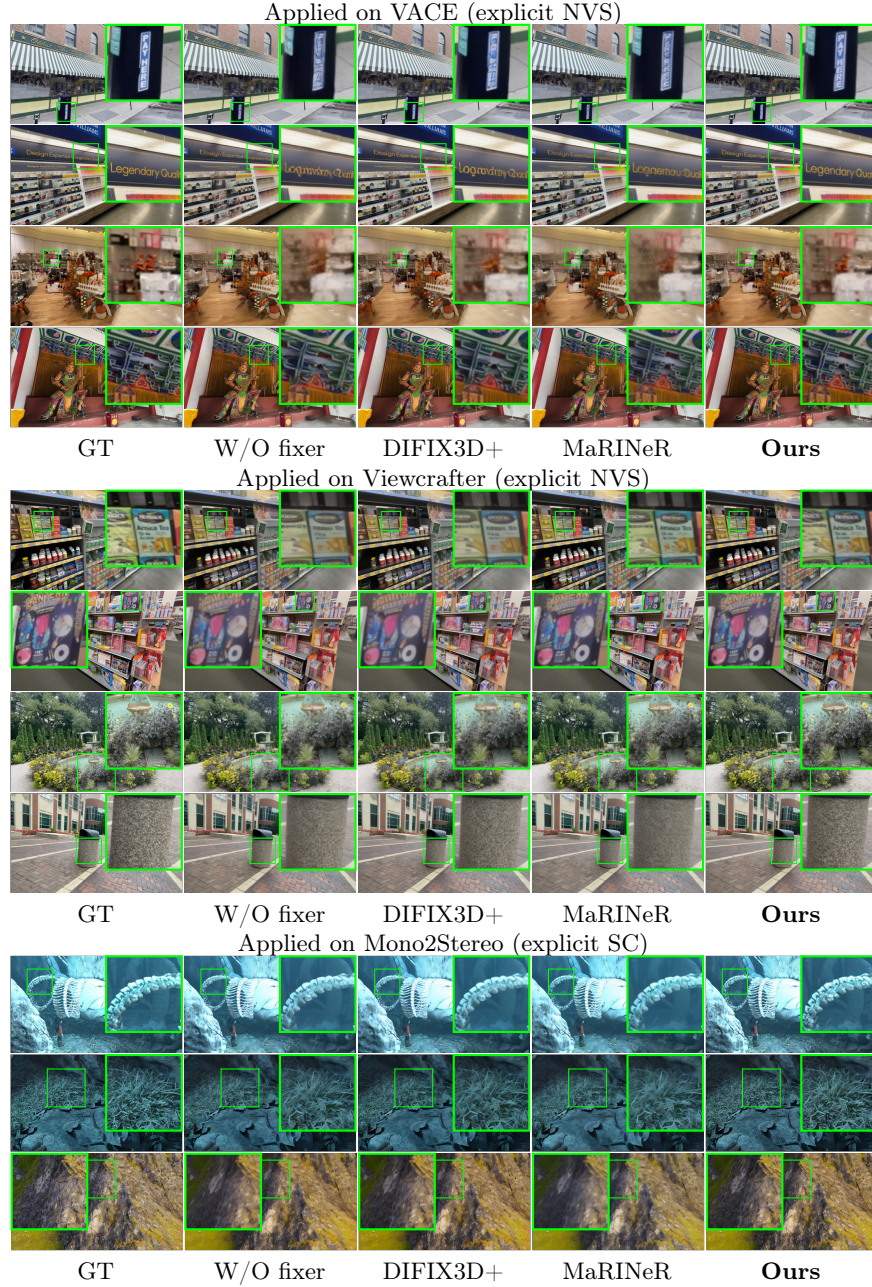


Fig. 12: Visual results of applying plug-and-play fixers (including DIFIX3D+ [48], MaRINeR [7], and ours) to improve diffusion-based view synthesis methods.

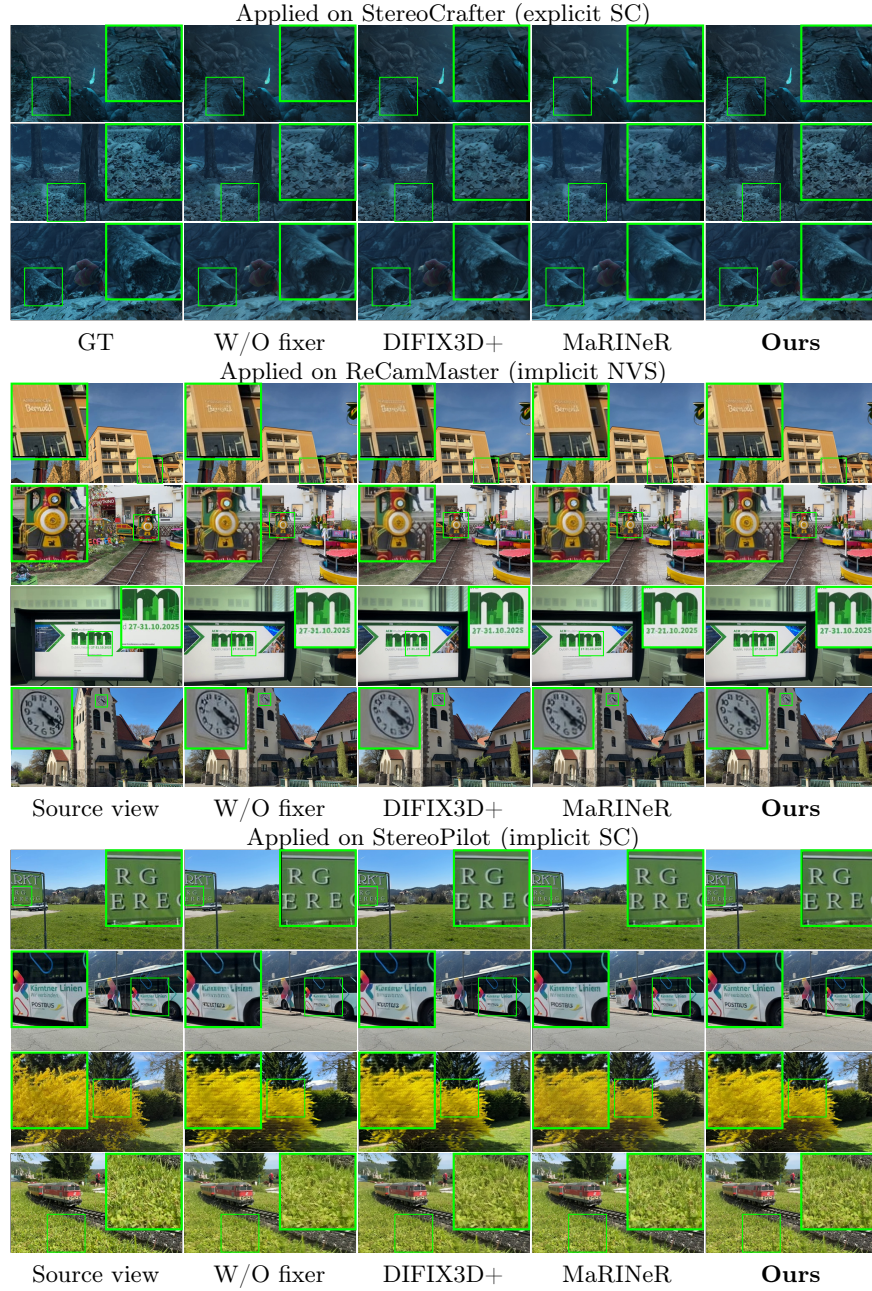


Fig. 12: Visual results of applying plug-and-play fixers (continued).

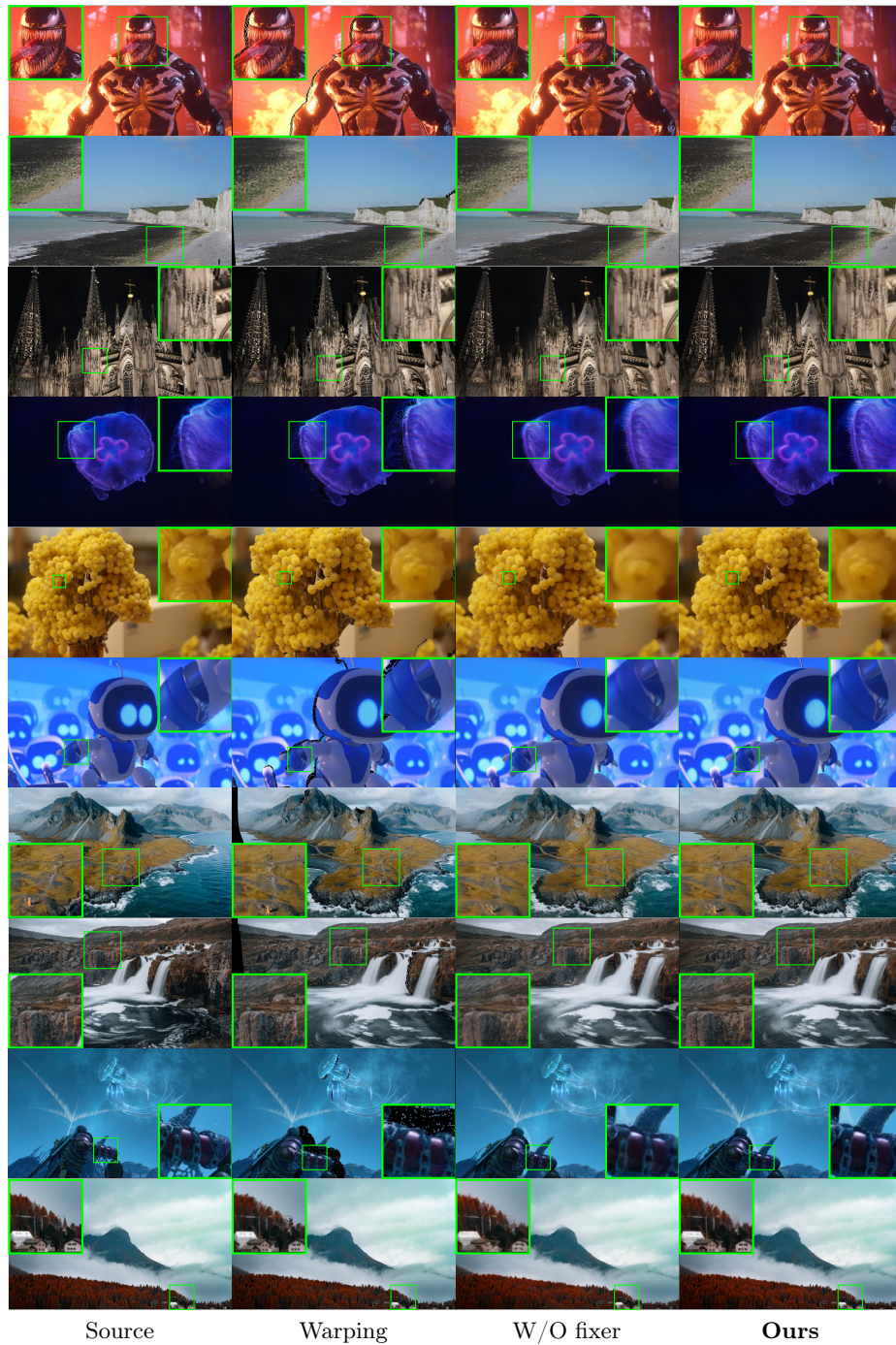


Fig. 13: Visual results of in-the-wild test.

References

1. An, J., Huang, S., Song, Y., Dou, D., Liu, W., Luo, J.: Artflow: Unbiased image style transfer via reversible neural flows. In: Proceedings of the IEEE/CVF conference on computer vision and pattern recognition. pp. 862–871 (2021)
2. Bahmani, S., Shen, T., Ren, J., Huang, J., Jiang, Y., Turki, H., Tagliasacchi, A., Lindell, D.B., Gojcic, Z., Fidler, S., et al.: Lyra: Generative 3d scene reconstruction via video diffusion model self-distillation. arXiv preprint arXiv:2509.19296 (2025)
3. Bai, J., Xia, M., Fu, X., Wang, X., Mu, L., Cao, J., Liu, Z., Hu, H., Bai, X., Wan, P., et al.: Recammaster: Camera-controlled generative rendering from a single video. In: Proceedings of the IEEE/CVF International Conference on Computer Vision. pp. 14834–14844 (2025)
4. Behrens, T., Obukhov, A., Ke, B., Tosi, F., Poggi, M., Schindler, K.: Stereospace: Depth-free synthesis of stereo geometry via end-to-end diffusion in a canonical space. arXiv preprint arXiv:2512.10959 (2025)
5. Bernasconi, M., Djelouah, A., Zhang, Y., Gross, M., Schroers, C.: Rebar: Reference-based image restoration. In: Proceedings of the IEEE/CVF International Conference on Computer Vision. pp. 5489–5498 (2025)
6. Blattmann, A., Dockhorn, T., Kulal, S., Mendeleevitch, D., Kilian, M., Lorenz, D., Levi, Y., English, Z., Voleti, V., Letts, A., et al.: Stable video diffusion: Scaling latent video diffusion models to large datasets. arXiv preprint arXiv:2311.15127 (2023)
7. Bösigler, L., Dusmanu, M., Pollefeys, M., Bauer, Z.: Mariner: Enhancing novel views by matching rendered images with nearby references. In: European Conference on Computer Vision. pp. 76–94. Springer (2024)
8. Cao, J., Liang, J., Zhang, K., Li, Y., Zhang, Y., Wang, W., Gool, L.V.: Reference-based image super-resolution with deformable attention transformer. In: European conference on computer vision. pp. 325–342. Springer (2022)
9. Chu, R., He, Y., Chen, Z., Zhang, S., Xu, X., Xia, B., Wang, D., Yi, H., Liu, X., Zhao, H., et al.: Wan-move: Motion-controllable video generation via latent trajectory guidance. arXiv preprint arXiv:2512.08765 (2025)
10. Dai, J., Qi, H., Xiong, Y., Li, Y., Zhang, G., Hu, H., Wei, Y.: Deformable convolutional networks (2017), <https://arxiv.org/abs/1703.06211>
11. Ding, K., Ma, K., Wang, S., Simoncelli, E.P.: Image quality assessment: Unifying structure and texture similarity. *IEEE Transactions on Pattern Analysis and Machine Intelligence* **44**(5), 2567–2581 (2022)
12. Dosovitskiy, A., Beyer, L., Kolesnikov, A., Weissenborn, D., Zhai, X., Unterthiner, T., Dehghani, M., Minderer, M., Heigold, G., Gelly, S., et al.: An image is worth 16x16 words: Transformers for image recognition at scale. arXiv preprint arXiv:2010.11929 (2020)
13. Fan, X., Girish, S., Ramanujan, V., Wang, C., Mirzaei, A., Sushko, P., Siarohin, A., Tulyakov, S., Krishna, R.: Omniview: An all-seeing diffusion model for 3d and 4d view synthesis (2025), <https://arxiv.org/abs/2512.10940>
14. Gao, R., Holynski, A., Henzler, P., Brussee, A., Martin-Brualla, R., Srinivasan, P., Barron, J.T., Poole, B.: Cat3d: Create anything in 3d with multi-view diffusion models. In: NeurIPS (2024)
15. Geyer, M., Tov, O., Jin, L., Tucker, R., Mosseri, I., Dekel, T., Snavely, N.: Eye2eye: A simple approach for monocular-to-stereo video synthesis. arXiv preprint arXiv:2505.00135 (2025)

16. He, H., Xu, Y., Guo, Y., Wetzstein, G., Dai, B., Li, H., Yang, C.: Cameractrl: Enabling camera control for text-to-video generation. arXiv preprint arXiv:2404.02101 (2024)
17. Heusel, M., Ramsauer, H., Unterthiner, T., Nessler, B., Hochreiter, S.: Gans trained by a two time-scale update rule converge to a local nash equilibrium. In: Advances in neural information processing systems. pp. 6626–6637 (2017)
18. Izadimehr, M., Ghanbari, M., Chen, G., Zhou, W., Hao, X., Dasari, M., Timmerer, C., Amirpour, H.: Svd: Spatial video dataset. In: Proceedings of the 33rd ACM International Conference on Multimedia. pp. 12988–12994 (2025)
19. Jiang, Z., Han, Z., Mao, C., Zhang, J., Pan, Y., Liu, Y.: Vace: All-in-one video creation and editing. In: Proceedings of the IEEE/CVF International Conference on Computer Vision. pp. 17191–17202 (2025)
20. Ju, X., Liu, X., Wang, X., Bian, Y., Shan, Y., Xu, Q.: Brushnet: A plug-and-play image inpainting model with decomposed dual-branch diffusion. In: European Conference on Computer Vision. pp. 150–168. Springer (2024)
21. Ke, B., Obukhov, A., Huang, S., Metzger, N., Daudt, R.C., Schindler, K.: Repurposing diffusion-based image generators for monocular depth estimation. In: Proceedings of the IEEE/CVF conference on computer vision and pattern recognition. pp. 9492–9502 (2024)
22. Ke, J., Wang, Q., Wang, Y., Milanfar, P., Yang, F.: Musiq: Multi-scale image quality transformer. In: Proceedings of the IEEE/CVF International Conference on Computer Vision. pp. 5148–5157 (2021)
23. Kingma, D.P., Ba, J.: Adam: A method for stochastic optimization. arXiv preprint arXiv:1412.6980 (2014)
24. Kingma, D.P., Welling, M.: Auto-encoding variational bayes. arXiv preprint arXiv:1312.6114 (2013)
25. Kolkin, N., Kucera, M., Paris, S., Sykora, D., Shechtman, E., Shakhnarovich, G.: Neural neighbor style transfer. arXiv preprint arXiv:2203.13215 (2022)
26. Liang, H., Cao, J., Goel, V., Qian, G., Korolev, S., Terzopoulos, D., Platanotis, K.N., Tulyakov, S., Ren, J.: Wonderland: Navigating 3d scenes from a single image. arXiv preprint arXiv:2412.12091 (2024)
27. Lin, H., Chen, S., Liew, J., Chen, D.Y., Li, Z., Shi, G., Feng, J., Kang, B.: Depth anything 3: Recovering the visual space from any views. arXiv preprint arXiv:2511.10647 (2025)
28. Ling, L., Sheng, Y., Tu, Z., Zhao, W., Xin, C., Wan, K., Yu, L., Guo, Q., Yu, Z., Lu, Y., et al.: D3dv-10k: A large-scale scene dataset for deep learning-based 3d vision. In: Proceedings of the IEEE/CVF Conference on Computer Vision and Pattern Recognition. pp. 22160–22169 (2024)
29. Lu, L., Li, W., Tao, X., Lu, J., Jia, J.: Masa-sr: Matching acceleration and spatial adaptation for reference-based image super-resolution. In: Proceedings of the IEEE/CVF Conference on Computer Vision and Pattern Recognition. pp. 6368–6377 (2021)
30. Van der Maaten, L., Hinton, G.: Visualizing data using t-sne. *Journal of machine learning research* **9**(11) (2008)
31. Mehl, L., Bruhn, A., Gross, M., Schroers, C.: Stereo conversion with disparity-aware warping, compositing and inpainting. In: WACV. pp. 4260–4269 (2024)
32. Mehl, L., Schmalfluss, J., Jahedi, A., Nalivayko, Y., Bruhn, A.: Spring: A high-resolution high-detail dataset and benchmark for scene flow, optical flow and stereo. In: Proceedings of the IEEE/CVF Conference on Computer Vision and Pattern Recognition. pp. 4981–4991 (2023)

33. Metzger, N., Truong, P., Bhat, G., Schindler, K., Tombari, F.: Elastic3d: Controllable stereo video conversion with guided latent decoding. arXiv preprint arXiv:2512.14236 (2025)
34. Niklaus, S., Liu, F.: Softmax splatting for video frame interpolation. In: Proceedings of the IEEE/CVF conference on computer vision and pattern recognition. pp. 5437–5446 (2020)
35. Peebles, W., Xie, S.: Scalable diffusion models with transformers. In: Proceedings of the IEEE/CVF international conference on computer vision. pp. 4195–4205 (2023)
36. Ren, X., Shen, T., Huang, J., Ling, H., Lu, Y., Nimier-David, M., Müller, T., Keller, A., Fidler, S., Gao, J.: Gen3c: 3d-informed world-consistent video generation with precise camera control. In: Proceedings of the IEEE/CVF Conference on Computer Vision and Pattern Recognition. pp. 6121–6132 (2025)
37. Ronneberger, O., Fischer, P., Brox, T.: U-net: Convolutional networks for biomedical image segmentation. In: International Conference on Medical image computing and computer-assisted intervention. pp. 234–241. Springer (2015)
38. Sauer, A., Lorenz, D., Blattmann, A., Rombach, R.: Adversarial diffusion distillation. In: European Conference on Computer Vision. pp. 87–103. Springer (2024)
39. Shen, G., Du, Y., Ge, W., He, J., Chang, C., Zhou, D., Yang, Z., Wang, L., Tao, X., Chen, Y.C.: Stereopilot: Learning unified and efficient stereo conversion via generative priors. arXiv preprint arXiv:2512.16915 (2025)
40. Shvetsova, N., Bhat, G., Truong, P., Kuehne, H., Tombari, F.: M2svid: End-to-end inpainting and refinement for monocular-to-stereo video conversion. arXiv preprint arXiv:2505.16565 (2025)
41. Siméoni, O., Vo, H.V., Seitzer, M., Baldassarre, F., Oquab, M., Jose, C., Khalidov, V., Szafraniec, M., Yi, S., Ramamonjisoa, M., et al.: Dinov3. arXiv preprint arXiv:2508.10104 (2025)
42. Sitzmann, V., Rezhikov, S., Freeman, B., Tenenbaum, J., Durand, F.: Light field networks: Neural scene representations with single-evaluation rendering. *Advances in Neural Information Processing Systems* **34**, 19313–19325 (2021)
43. Wan, T., Wang, A., Ai, B., Wen, B., Mao, C., Xie, C.W., Chen, D., Yu, F., Zhao, H., Yang, J., et al.: Wan: Open and advanced large-scale video generative models. arXiv preprint arXiv:2503.20314 (2025)
44. Wang, J., Chan, K.C., Loy, C.C.: Exploring clip for assessing the look and feel of images. In: Proceedings of the AAAI Conference on Artificial Intelligence. vol. 37, pp. 2555–2563 (2023)
45. Wang, L., Frisvad, J.R., Jensen, M.B., Bigdeli, S.A.: Stereodiffusion: Training-free stereo image generation using latent diffusion models. In: Proceedings of the IEEE/CVF Conference on Computer Vision and Pattern Recognition. pp. 7416–7425 (2024)
46. Wang, Y., Lipson, L., Deng, J.: Sea-raft: Simple, efficient, accurate raft for optical flow. In: European Conference on Computer Vision. pp. 36–54. Springer (2024)
47. Wang, Z., Bovik, A.C., Sheikh, H.R., Simoncelli, E.P.: Image quality assessment: from error visibility to structural similarity. *IEEE Transactions on Image Processing* **13**(4), 600–612 (2004)
48. Wu, J.Z., Zhang, Y., Turki, H., Ren, X., Gao, J., Shou, M.Z., Fidler, S., Gojcic, Z., Ling, H.: Difix3d+: Improving 3d reconstructions with single-step diffusion models. In: Proceedings of the Computer Vision and Pattern Recognition Conference. pp. 26024–26035 (2025)
49. Xing, K., Jin, X., Li, L., Yin, Y., Liang, H., Luo, G., Fang, C., Wang, J., Plataniotis, K.N., Zhao, Y., et al.: Stereoworld: Geometry-aware monocular-to-stereo video generation. arXiv preprint arXiv:2512.09363 (2025)

50. Yang, L., Kang, B., Huang, Z., Zhao, Z., Xu, X., Feng, J., Zhao, H.: Depth anything v2. *Advances in Neural Information Processing Systems* **37**, 21875–21911 (2024)
51. Yang, S., Wu, T., Shi, S., Lao, S.s., Gong, Y., Cao, M., Wang, J., Yang, Y.: Maniqa: Multi-dimension attention network for no-reference image quality assessment. In: *Proceedings of the IEEE/CVF conference on computer vision and pattern recognition workshops*. pp. 1190–1199 (2022)
52. Yoo, J., Uh, Y., Chun, S., Kang, B., Ha, J.W.: Photorealistic style transfer via wavelet transforms. In: *Proceedings of the IEEE/CVF international conference on computer vision*. pp. 9036–9045 (2019)
53. Yu, S., Chen, Y., Qi, Z., Xie, Z., Wang, Y., Wang, L., Shan, Y., Lu, H.: Mono2stereo: A benchmark and empirical study for stereo conversion. In: *Proceedings of the Computer Vision and Pattern Recognition Conference*. pp. 21847–21856 (2025)
54. Yu, W., Xing, J., Yuan, L., Hu, W., Li, X., Huang, Z., Gao, X., Wong, T.T., Shan, Y., Tian, Y.: Viewcrafter: Taming video diffusion models for high-fidelity novel view synthesis. *arXiv preprint arXiv:2409.02048* (2024)
55. Zhang, R., Isola, P., Efros, A.A., Shechtman, E., Wang, O.: The unreasonable effectiveness of deep features as a perceptual metric. In: *Proceedings of the IEEE conference on computer vision and pattern recognition*. pp. 586–595 (2018)
56. Zhang, X., Ke, B., Riemenschneider, H., Metzger, N., Obukhov, A., Gross, M., Schindler, K., Schroers, C.: Betterdepth: Plug-and-play diffusion refiner for zero-shot monocular depth estimation. *Advances in Neural Information Processing Systems* **37**, 108674–108709 (2024)
57. Zhang, X., Zhang, Y., Mehl, L., Gross, M., Schroers, C.: High-fidelity novel view synthesis via splatting-guided diffusion. In: *Proceedings of the Special Interest Group on Computer Graphics and Interactive Techniques Conference Conference Papers*. pp. 1–11 (2025)
58. Zhang, X., Zhang, Y., Mehl, L., Gross, M., Schroers, C.: Guardians of the hair: Rescuing soft boundaries in depth, stereo, and novel views. In: *Proceedings of the Computer Vision and Pattern Recognition Conference* (2026)
59. Zhao, S., Hu, W., Cun, X., Zhang, Y., Li, X., Kong, Z., Gao, X., Niu, M., Shan, Y.: Stereocrafter: Diffusion-based generation of long and high-fidelity stereoscopic 3d from monocular videos. *arXiv preprint arXiv:2409.07447* (2024)
60. Zhou, J., Gao, H., Voleti, V., Vasishta, A., Yao, C.H., Boss, M., Torr, P., Rupprecht, C., Jampani, V.: Stable virtual camera: Generative view synthesis with diffusion models. In: *Proceedings of the IEEE/CVF International Conference on Computer Vision*. pp. 12405–12414 (2025)